Identification of mechanical properties in brushless permanent magnet motors by means of coil impedance measurement

T. Kimpián, F. Augusztinovicz
Budapest University of Technology and Economics Department of Telecommunication, Laboratory of Acoustics
Magyar Tudósok körútja 2., H-1117, Budapest, Hungary
email: **kimpian@hit.bme.hu**

Abstract
In this paper we present a new vibroacoustic and electro-mechanical coupled lumped equivalent network, which accurately describes torsional vibration conditions of permanent magnet synchronous motors (PMSMs) in case of single-phase pulsating current excitation in conjunction with small angular displacement of the rotor. Our model contains both mechanical and electrical parameters of the motor and yields their dependence upon rotor position and explains vibroacoustical effect of cogging torque. We introduce an experimental technique for the measurement of quantities proportional to mechanical and electrical impedance of the motor, than we provide a method for curve fitting and parameter identification on the measured transfer functions. Finally we present a case study on the detection of possible faults when cementation of the rotor magnets is not satisfactory.

1 Vibroacoustic model of an ideal permanent magnet synchronous machine

There are several methods for analyzing torsional systems in literature [1] [2] [3], and measurement techniques of these systems are also commonly available [1] [2]. In case of translational mechanical systems (like a loudspeaker) the use of lumped equivalent networks is a frequently applied approach too [4] [5] [6]. One example can be the classical loudspeaker box design [4] [5] [6], which requires an accurate model of magnetic circuitry of the loudspeaker as an electro-mechanical transducer. The most common task if one analyzes torsional systems is to reveal the vibration conditions under normal operating conditions and excitations.

The lumped equivalent electric network of permanent magnet synchronous motors (PMSMs) describes accurately the behavior of a motor when it is rotating at synchronous rotational speed n_0 [7]. However, predictions of this model can not be adopted directly when the stator is excited by a single phase non-sinusoidal current, instead of the conventional three-phase one.

In this paper first we present a linear coupled vibroacoustic lumped equivalent network which explains the interior processes of an ideal PMSM during single phase arbitrary current excitation (like white noise), when the angular rotation of the motor shaft is small enough to neglect changes in the magnetic conditions of the motor.

In order to come out with a reliably applicable motor model we have to take into account the vibroacoustic effect of the so called cogging torque of a PMSM. However, while cogging torque is a well known phenomenon in machine construction and its reduction is essential in high performance drive applications [7] [8] [9], the vibroacoustic aspects of it is still undiscovered. In the 2nd chapter we introduce a possible

modeling approach that allows to use a simple lumped equivalent component in the torsional vibroacoustic model.

1.1 Derivation of the motor model

Building up a motor model one can regard the following. The well-known equivalent electric network (Figure 1) depicts the processes in the motor at n_0 synchronous rotational speed, by using complex voltages and currents. R and L mean the Ohmic resistance and inductance of the stator, respectively, $\underline{U}$ means complex induced voltage (which is proportional to the angular velocity of the rotor), and $\underline{U}_p$, $\underline{I}_p$ mean the complex phase voltage and phase current, respectively.

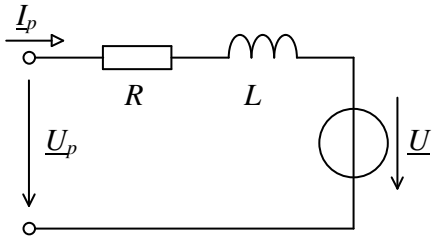

Figure 1: Equivalent network of a synchronous machine

Let us continue the investigations by assuming one-phase random current supply rather than the standard three-phase excitation. As a result, the rotor will vibrate torsionally around an equilibrium position instead of constant rotation.

In order to adopt the model to this pulsating field excitation, one has to examine, which of these parameters are the function of the φ mechanical angle between the rotor and the stator.

The DC resistance R obviously does not depend on the position of the rotor, while it is not true for inductance and induced voltage, hence let us have $L(\varphi)$ and $u(\varphi)$ position dependent quantities. The instantaneous value of inductance depends on the condition of the magnetic circuitry, which changes according to the angle between the rotor and the stator. If the angular displacement is small indeed, inductance can be regarded as a constant in a given position.

For the expression of the induced voltage and the current flowing in the winding, let us examine, what happens with an ideal conductor frame placed in a homogenous magnetic field $\underline{B}$!

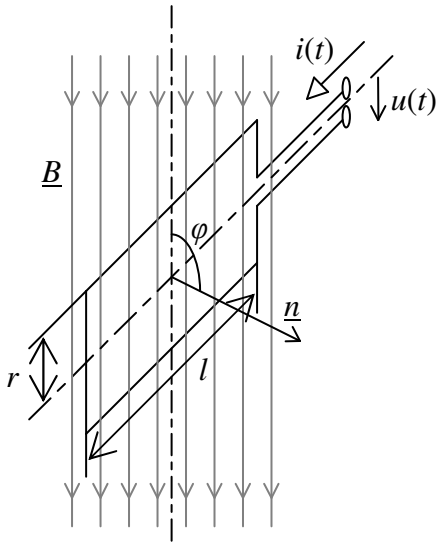

Figure 2: Ideal conductor frame placed in a homogenous magnetic field

According to Faraday's law of induction, the induced voltage in the conductor frame ($u(t)$) will be proportional to the induction (B), linear sizes of the frame (r, l), the angular velocity of the rotation ($\theta(t)$) and the rotation angle between the normal of the frame and the field ($\sin(\varphi)$):

$$u(t) = \theta(t) Blr \sin(\varphi) \tag{1}$$

Similarly, if current ($i(t)$) flows in the ideal conductor frame, the torque acting on the frame (($m(t)$) can be described as follows:

$$m(t) = i(t) Blr \sin(\varphi) \tag{2}$$

These equations hold if the angular displacement of the rotor is small enough.

Though the ideal conductor frame placed in a homogenous field is a rather simple model of a real motor, it represents the physical processes in an appropriate way, therefore equations (1) and (2) can be applied in case of a two-pole machine as well. If the machine in question has $2p$ poles, $p\varphi$ should be written in place of φ.

Note that the constants and $\sin(\varphi)$ indicated in Equations (1) and (2) may be contracted to a rotor position (φ) dependent electromagnetic transmission parameter, and thus the motor can be handled as an ideal torsional electromagnetic transducer. The Equations connecting the electrical and mechanical sides may thus be expressed in the following form:

$$u(t) = \theta(t) T(\varphi) \tag{3}$$

$$m(t) = i(t) T(\varphi) \tag{4}$$

where $T(\varphi)$ denotes the (angle dependent) electromagnetic transmission ratio.

Equations (3) and (4) enable one to draw the lumped equivalent circuit as depicted in Figure 3 by using the analogies applicable on torsional and mechanic systems (see Table 1 below).

Translation			Torsion		
Displacement	$x(t)$	[m]	Angular displacement	$\varphi(t)$	[rad]
Velocity	$v(t)$	[m/s]	Angular velocity	$\theta(t)$	[rad/s]
Acceleration	$a(t)$	[m/s^2]	Angular acceleration	$\beta(t)$	[rad/s^2]
Force	$f(t)$	[N]	Torque	$m(t)$	[Nm]
Mass	M	[kg]	Moment of inertia	J	[kgm^2]
Compliance	C_d	[m/N]	Torsional compliance	C_m	[rad/Nm]
Mechanical resistance	R_d	[Ns/m]	Torsional resistance	R_m	[Nms/rad]

Table 1: Analogies between translational and torsional systems

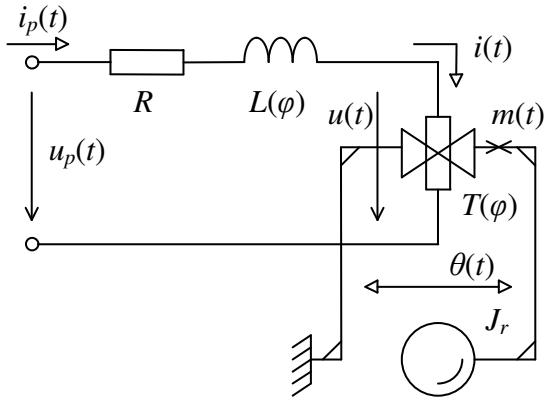

Figure 3: Lumped equivalent network of the ideal permanent magnet synchronous machine valid for pulsating current excitation

1.2 Calculation of impedance curve of an ideal PMSM

Let us express the electrical impedance of a motor on the basis of the equivalent network of Figure 3. Hereafter we will use Laplace-transforms instead of time functions according to the following definition:

$$X(s) = \int_0^\infty x(t)e^{-st}dt \tag{5}$$

Let us first examine, how the electro-mechanical transducer transforms electrical and mechanical impedances. Inserting Laplace-transforms of Equations (3) and (4) to the expression of electrical impedance, we get the following equation:

$$Z_{em}(s) = \frac{U(s)}{I(s)} = \frac{\Theta(s)T(\varphi)}{\frac{M(s)}{T(\varphi)}} = T^2(\varphi)\frac{\Theta(s)}{M(s)} = \frac{T^2(\varphi)}{Z_m(s)} \tag{6}$$

During the deduction we introduced the term of torsional mechanical impedance $Z_m(s)$ (a useful concept in description of torsional systems) which is simply the quotient of torque and angular velocity.

As one can see, the motor transforms the impedance from one side to the other reciprocally, multiplied by the square of the transmission ratio. Using this relationship, we can derive the electric equivalent of the moment of inertia (J_r) of the rotating part of the motor, resulting in a condenser of capacitance $J_r/T^2(\varphi)$ (Figure 4).

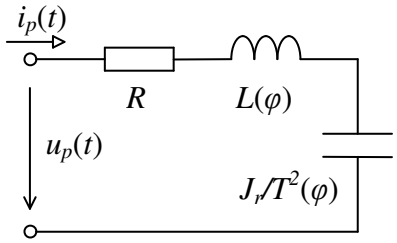

Figure 4: Electrical vibroacoustic equivalent network of ideal synchronous machine

Therefore the electrical side impedance can be described as follows:

$$Z_e(s) = \frac{U_p(s)}{I_p(s)} = R + sL(\varphi) + \frac{1}{s\frac{J_r}{T^2(\varphi)}} = \frac{T^2(\varphi) + sRJ_r + s^2J_rL(\varphi)}{sJ_r} \tag{7}$$

Note that the formula is equivalent to the impedance of a series RLC circuit. If we consider the expression as a transfer function, we face a problem since real physical systems may not have a transfer function which has a polynomial of higher degree of freedom in s in the denominator than that of the numerator. This contradiction arises from the fact that we did not pay attention to the stray capacities of the coils during the construction of the model, which obviously influences the high frequency behavior of the impedance curve fundamentally. A possible and simple workabout is to consider electrical admittance rather than impedance:

$$Y_e(s) = \frac{I_p(s)}{U_p(s)} = \frac{sJ_r}{T^2(\varphi) + sRJ_r + s^2J_rL(\varphi)} \tag{8}$$

In this case the undamped natural frequency and damping factor of the complex-conjugated pole-pair indicated in the expression of admittance may be expressed in the following form:

$$\omega_0 = \frac{1}{\sqrt{\frac{J_r}{T^2(\varphi)} L(\varphi)}} = \frac{T(\varphi)}{\sqrt{J_r L(\varphi)}} \tag{9}$$

and

$$\xi = \frac{R}{2}\sqrt{\frac{\frac{J_r}{T^2(\varphi)}}{L(\varphi)}} = \frac{R}{2T(\varphi)}\sqrt{\frac{J_r}{L(\varphi)}} \tag{10}$$

2 Vibroacoustic model of a non-ideal PMSM

2.1 Derivation of the non-ideal motor model

In the previous section we have introduced the vibroacoustic model of an ideal permanent magnet synchronous machine, which contains the moment of inertia of the rotating part, and the electro-mechanical transducer describing the connection between the mechanical and electrical features of the motor.

However, to rotate the shaft of a real permanent magnet synchronous machine a nonzero torque is required, even if no current is fed to the winding (i.e., the electric excitation of the system is zero). This torque is the result of the torque considered as proportional with the angular velocity caused by friction and other (e.g. magnetic) losses on one side, and of the so called cogging torque arising from the irregularity of the magnetic field of the motor on the other.

The torque component being proportional to the angular velocity may be taken into account by a torsional mechanical damping element (see R_m in figure), however, the modeling of the effect of the cogging torque requires further considerations.

Let us assume that the cogging torque varies as a cosine function of the angle, if no electric excitation is applied:

$$M_c = \hat{M}\cos(p\varphi) \tag{11}$$

In Figure 5 one can see an example, where theoretical cogging torque of a four-pole machine is represented.

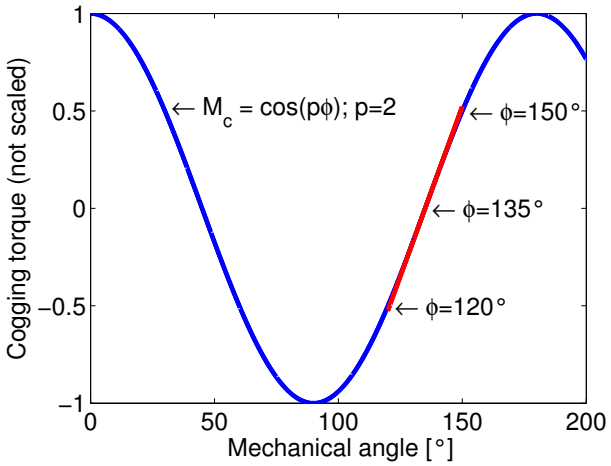

Figure 5: Theoretical cogging torque as a function of the angle in case of a four-pole machine

Constraining now our investigations to small angles of rotation around the stable positions of the rotor (i.e. where the cogging torque is close to zero), the cosine curve can be substituted by a linear function. This means that the cogging torque can be allowed for in the equivalent network by a spring of torsional compliance $C_m(\varphi)$, being a function of rotor position too. Figure 6 shows the equivalent network extended by these two new components:

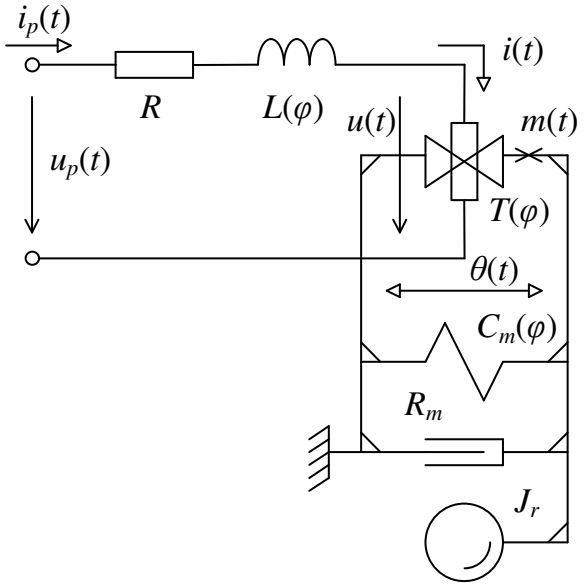

Figure 6: Vibroacoustic model of a non-ideal permanent magnet synchronous machine

2.2 Calculation of impedance curve of a non-ideal PMSM

The expression of the impedance on the electric side can be calculated from this equivalent network as well. For this, the resulting impedance of the elements on the mechanical side should be determined first:

$$Z_{em}(s) = \frac{T^2(\varphi)}{Z_m(s)} = \frac{sT^2(\varphi)C_m(\varphi)}{1 + sR_mC_m(\varphi) + s^2J_rC_m(\varphi)} \tag{12}$$

where

$$Z_m(s) = \frac{1}{sC_m(\varphi)} + R_m + sJ_r = \frac{1 + sR_mC_m(\varphi) + s^2J_rC_m(\varphi)}{sC_m(\varphi)} \tag{13}$$

If we add the impedance of the electric elements, we get the equation below (note that we have omitted angle dependence for the sake of simplicity):

$$Z_e(s) = R + sL + Z_{em}(s) = \frac{R + s(C_mR_mR + L + T^2C_m) + s^2C_m(J_rR + R_mL) + s^3J_rC_mL}{1 + sC_mR_m + s^2J_rC_m} \tag{14}$$

Similarly to the ideal model, we continue with the expression of the admittance:

$$Y_e(s) = \frac{1 + sC_mR_m + s^2J_rC_m}{R + s(C_mR_mR + L + T^2C_m) + s^2C_m(J_rR + R_mL) + s^3J_rC_mL} \tag{15}$$

For the calculation of the undamped natural frequencies we disregard the losses in (15), i.e. we insert $R = 0$ and $R_m = 0$:

$$Y_e(s) = \frac{1 + s^2 J_r C_m}{s(L + T^2 C_m) + s^3 J_r C_m L} = \frac{1}{s(L + T^2 C_m)} \frac{1 + s^2 J_r C_m}{1 + s^2 \frac{J_r C_m L}{L + T^2 C_m}} \tag{16}$$

From Equation (16) one can estimate the natural frequencies of undamped poles and zeros as follows:

$$\omega_p = \frac{1}{\sqrt{\frac{J_r C_m L}{L + T^2 C_m}}} = \sqrt{\frac{L + T^2 C_m}{J_r C_m L}} \tag{17}$$

and

$$\omega_z = \frac{1}{\sqrt{J_r C_m}} \tag{18}$$

Generally speaking one can draw the conclusion that any kind of components on the mechanical side of a motor affect the impedance as measured on the electrical side as well. This statement is really important, as it suggests that one can determine the mechanical loading impedance, attached to the shaft of the motor, from electrical impedance measurement, provided that an appropriate electro-mechanical model of the motor is available.

3 Identification of model parameters with measured transfer functions

In order to validate of the vibroacoustic model developed in Chapter 2 and to identify model parameters, one should measure both electric and mechanical impedances. In this chapter we review the applied measurement methods and show, how one can fit transfer functions to the results of those measurements. It will also be demonstrated, how model parameters can be matched to the parameters of fitted transfer functions, and eventually results obtained from the identification of a ten-pole PMSM will be presented.

3.1 Measurement methods of mechanical and electrical impedance

If one uses the direct definition of the torsional mechanical impedance, the torque acting on the rotor for a known angular velocity is to be determined. As the measurement of torque needs rather complex instrumentation, it is very likely that it can not be fulfilled without altering normal torsional conditions of the motor. As a result, the direct measurement of mechanical impedance can most probably be used with proper foresight only for the validation of the motor model.

However, the motor model itself can be used for the measurement: as Equation (4) states that the torque is proportional to the current of the stator, by determining the current flowing across the motor we get a quantity which is proportional to the torque.

The measurement of angular velocity by using conventional methods is rather challenging. Utilizing a special test setup (see Figure 7) however, tangential acceleration of the rotor can be determined by applying simple tools, provided that the motor is fed by AC current of relatively high frequency. As a consequence, rather then rotating normally, the rotor will only oscillate with small rotational amplitudes around its stable position determined by zero cogging torque. Another benefit of this measurement setup is that the accelerometer mounted on the shaft loads the torsional system minimally.

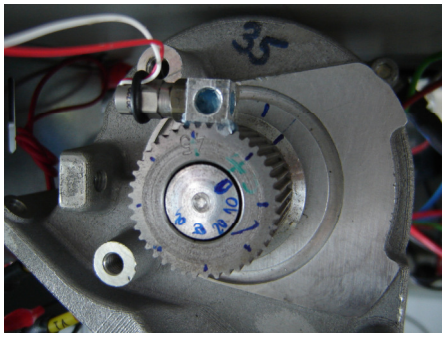

Figure 7: Test setup for measuring tangential acceleration of the motor shaft

Finally, the angular acceleration of the torsional system can be calculated as the quotient of measured tangential acceleration and corrected radius between shaft and accelerometer axis.

Now we should determine the relationship between mechanical impedance $H_m(s)=\beta(s)/I(s)$ and the transfer function measured by the method mentioned above:

$$H_m(s)=\frac{\beta(s)}{I_p(s)}=\frac{s\theta(s)}{\frac{M(s)}{T(\varphi)}}=sT(\varphi)\frac{\theta(s)}{M(s)}=sT(\varphi)\frac{1}{Z_m(s)} \tag{19}$$

In order to get the final result, let us insert the mechanical impedance gained from the non-ideal transducer model (Equation 13) into Equation (19):

$$H_m(s)=sT(\varphi)\frac{1}{\frac{1+sR_mC_m(\varphi)+s^2J_rC_m(\varphi)}{sC_m(\varphi)}}=\frac{s^2T(\varphi)C_m(\varphi)}{1+sR_mC_m(\varphi)+s^2J_rC_m(\varphi)} \tag{20}$$

This expression has many advantages. First, Equation (20) describes a stable system (a second order high-pass filter), therefore the model parameters can be estimated easily. On the other hand, beyond the electromagnetic transmission $T(\varphi)$ it contains only mechanical parameters of the motor.

In practice, we fed the stator by an audio current generator, recorded the voltage and current signals and angular acceleration by using a multichannel data acquisition system. According to Chapter 2.2, instead of electrical impedances we calculated electrical admittances from the recorded signals:

$$H_e(s)=Y_e(s)=\frac{I_p(s)}{U_p(s)} \tag{21}$$

3.2 Transfer function estimation and parameter identification

We fitted curves on both transfer functions: to $H_m(s)$ related to mechanical impedance and also to $H_e(s)$, which is equal to electrical admittance, by using the MATLAB S*ystem Identification Toolbox* (Ident). We estimated the parameters of the Output Error (OE) model (minimizing the difference between identified and original system's output signals) in the frequency domain [10].

As in Ident OE models the leading coefficient of denominator is equal to 1, one can express the transfer functions in the following forms:

$$H_m(s)=\frac{s^2T(\varphi)C_m(\varphi)}{1+sR_mC_m(\varphi)+s^2J_rC_m(\varphi)}=\frac{D(s)}{C(s)}=\frac{d_1+d_2s+d_3s^2}{c_1+c_2s+s^2}=\frac{D_1+D_2s+D_3s^2}{1+C_2s+C_3s^2} \tag{22}$$

$$H_e(s) = \frac{1 + sC_m R_m + s^2 J_r C_m}{R + s(C_m R_m R + L + T^2 C_m) + s^2 C_m (J_r R + R_m L) + s^3 J_r C_m L} =$$

$$= \frac{B(s)}{A(s)} = \frac{b_1 + b_2 s + b_3 s^2}{a_1 + a_2 s + a_3 s^2 + s^3} = \frac{1 + B_2 s + B_3 s^2}{A_1 + A_2 s + A_3 s^2 + A_4 s^3} \tag{23}$$

We should realize that in both cases the number of estimated parameters is fewer by one than the unknowns to be determined. A possible explanation is that knowledge of the natural frequency of an undamped resonant system does not contain enough information about the parameter values of the system. This means that all the unknowns of the system can be calculated only if one is given. Here it is most efficient if one chooses the moment of inertia of the rotor as the given value, since it occurs in both models and does not depend on φ. Therefore the following equations yield the relationships between the transfer functions and model parameters:

model parameters on the basis of $H_m(s)$:

$$T(\varphi) = \frac{D_3}{C_3} J_r,\ C_m(\varphi) = \frac{C_3}{J_r},\ R_m = \frac{C_2}{C_3} J_r \tag{24) (25) (26}$$

model parameters on the basis of $H_e(s)$:

$$R = A_1,\ L(\varphi) = \frac{A_4}{B_3},\ T(\varphi) = \sqrt{\frac{J_r}{B_3}\left(A_2 - A_1 B_2 - \frac{A_4}{B_3}\right)}, \tag{27) (28}$$

$$C_m(\varphi) = \frac{B_3}{J_r},\ R_m = \frac{B_2 J_r}{B_3} \tag{29) (30}$$

3.3 Display of identified parameters

The presented method was validated for a ten-pole PMSM. Figures 8 and 9 present the measured and estimated $H_m(s)$ and $H_e(s)$ transfer functions, respectively, in four rotor positions.

We checked the linearity of motor model on the basis of coherence functions for both $H_m(s)$ and $H_e(s)$ (Figure 10). Small displacements and the corresponding linearity assumed at the construction of the motor model are convincingly confirmed. (The noisiness of the coherence function corresponding to $H_m(s)$ at rotor position 13.1707 ° will be explained later.).

The identified parameters common to both $H_m(s)$ and $H_e(s)$ are summarized in Figure 11. Electromagnetic transmission, torsional compliance and torsional resistance are drawn as a function of the rotor position. The sinusoidal shape of the electromagnetic transmission and periodic changes of the compliance and resistance according to the number of poles can be readily observed. The electromagnetic transmission estimated from $H_e(s)$ slightly differs from the one estimated from $H_m(s)$, which can be explained by Equation (28): $T(\varphi)$ is square root of an algebraic expression, therefore we gained the absolute value of $T(\varphi)$, as compared to the foregoing.

Figure 12 presents electrical parameters identified from transfer functions $H_e(s)$. Measurement and identification uncertainties cause some position dependence in the calculated electrical resistance, and in accordance with previous expectations, the inductance shows sinusoidal dependence vs rotor position.

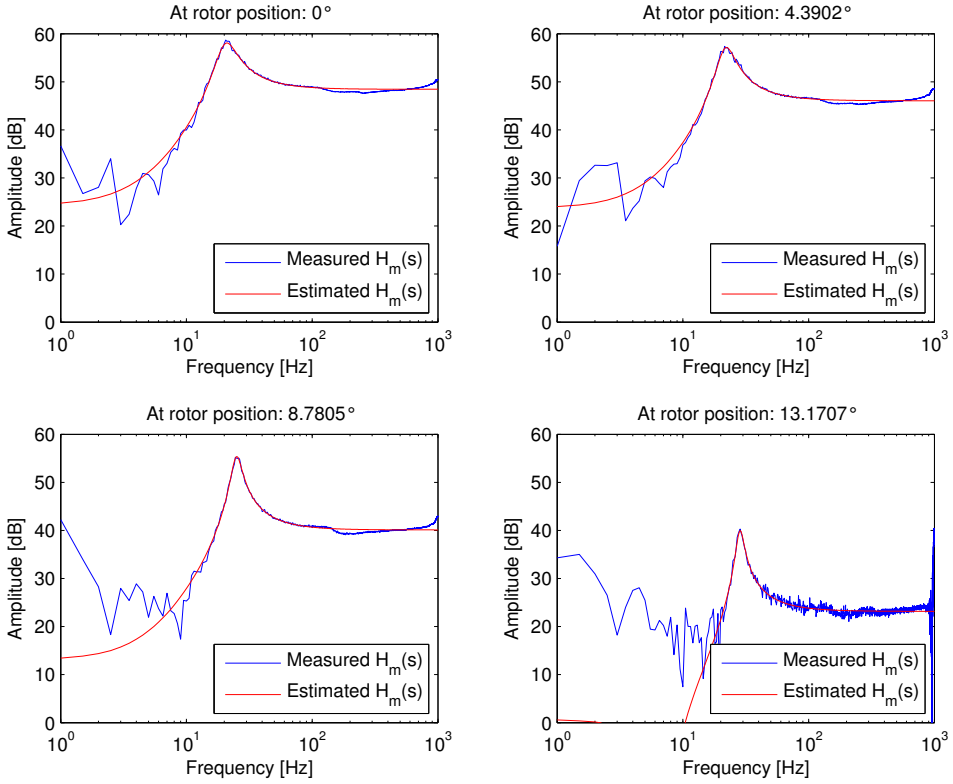

Figure 8: Measured and estimated transfer functions $H_m(s)$ for various rotor positions

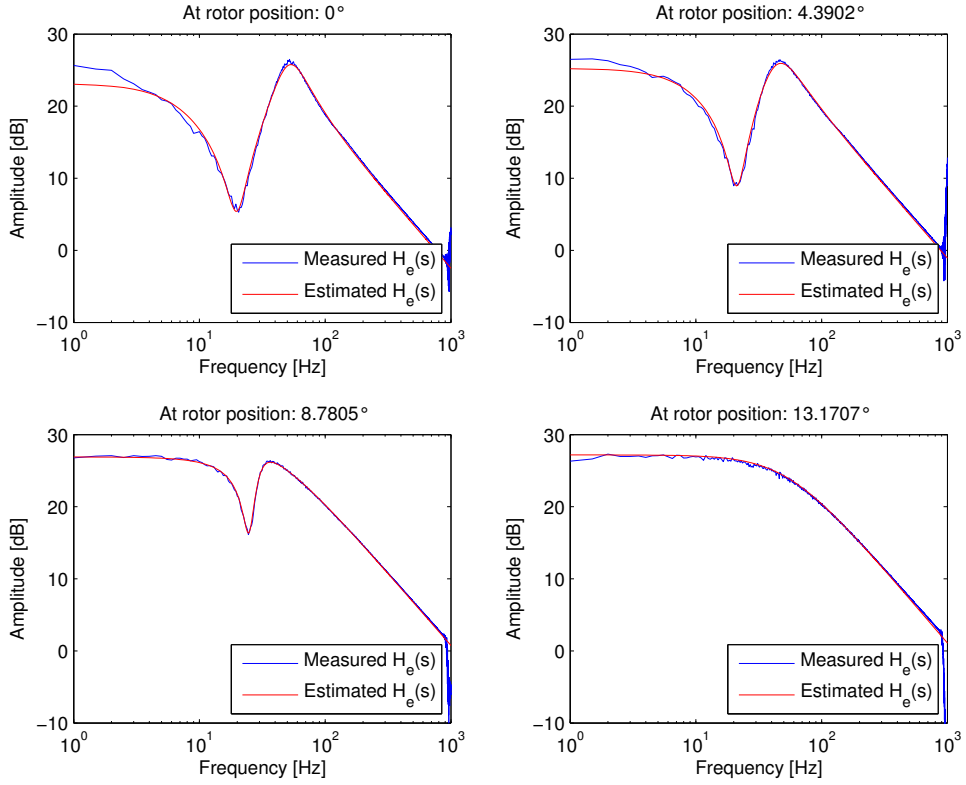

Figure 9: Measured and estimated transfer functions $H_e(s)$ for various rotor positions

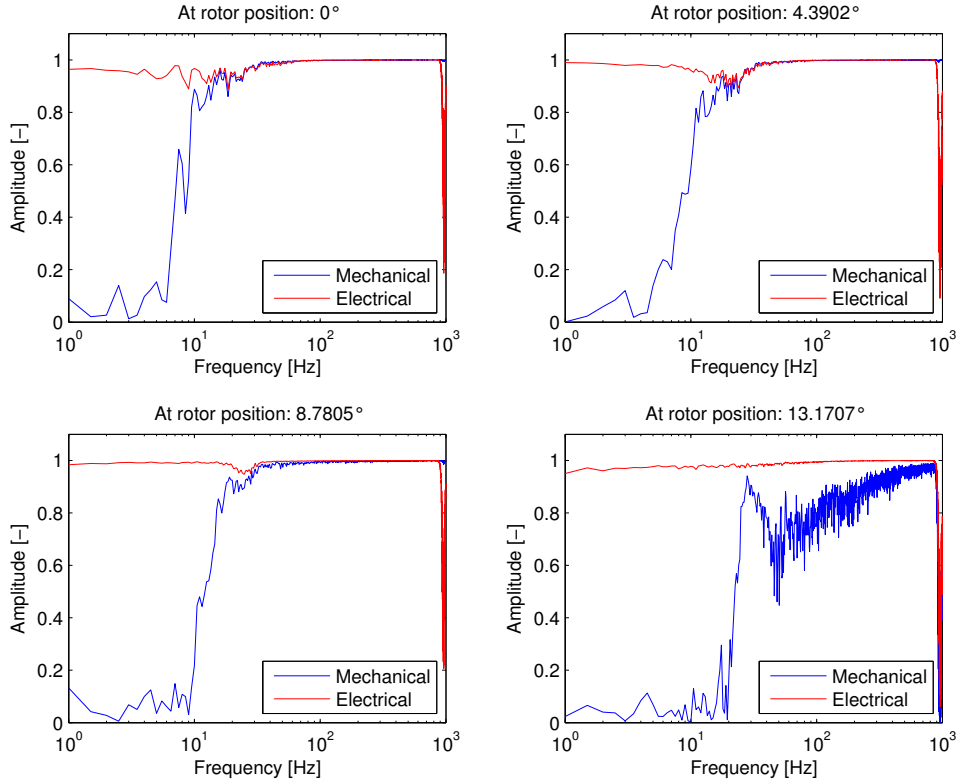

Figure 10: Measured coherence functions of $H_m(s)$ and $H_e(s)$ estimations for various rotor positions

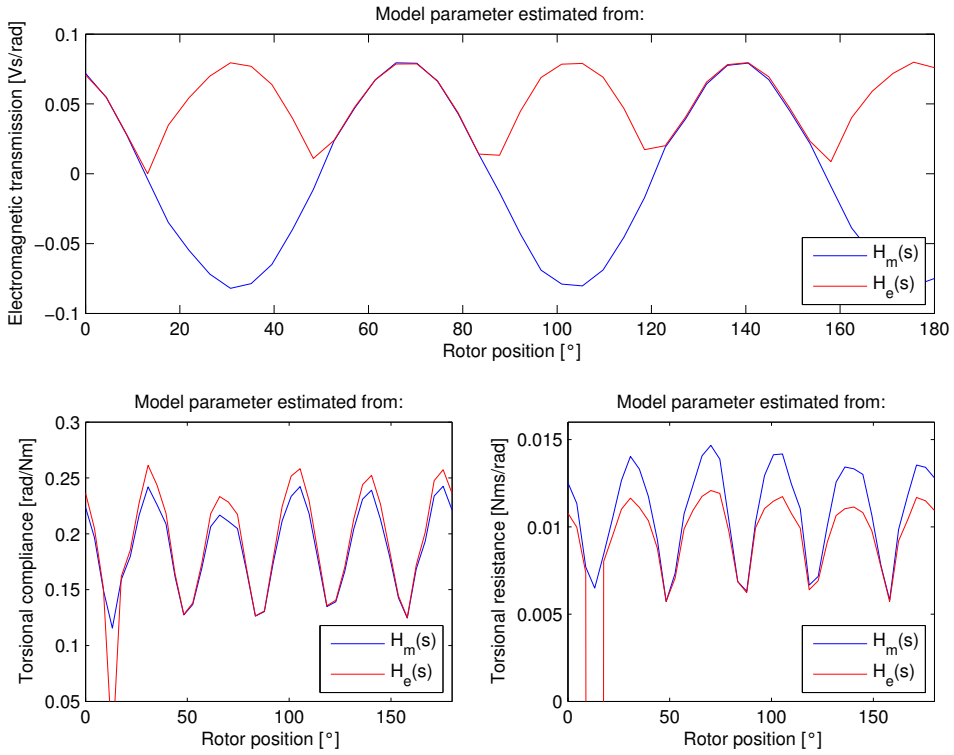

Figure 11: Estimated parameters common to transfer functions $H_m(s)$ and $H_e(s)$ for various rotor positions

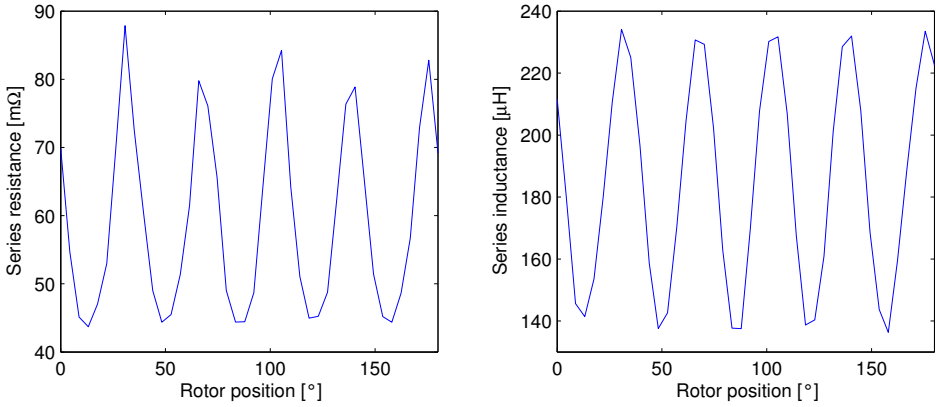

Figure 12: Electrical parameters estimated from transfer functions $H_e(s)$ for various rotor positions

Having estimated the electromagnetic transmission curve, we can now explain the noisiness of the coherence function of $H_m(s)$ for rotor position 13.1707°. The reason is very simple: the electromagnetic transmission in that rotor position is very close to zero, therefore hardly any energy can be transferred to the mechanical side, resulting in poor signal-to-noise ratio and coherence.

This simple, however substantial example shows, that when using this motor model for everyday problem solving, one should permanently keep in mind that the estimated model parameters are angular position dependent.

4 Mechanical analysis of a typical rotor of a PMSM

Hereafter we present some finite element simulation results, made by means of ANSYS Workbench 11. Figure 13 shows a possible mechanical construction of the rotor of a PMSM. For the nominal rotational speed range, that kind of rotor can be considered as a rigid body, but from a vibroacoustic point of view, the bridges between the shaft and poles cannot be considered to have infinite stiffness (Figure 14).

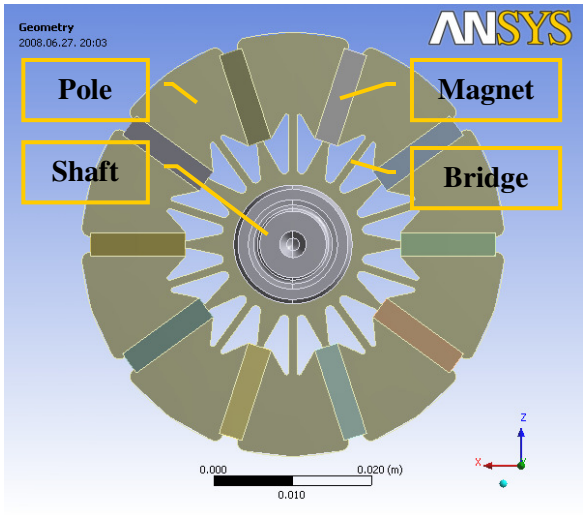

Figure 13: Sketch of a possible mechanical construction of rotor of a ten-pole PMSM

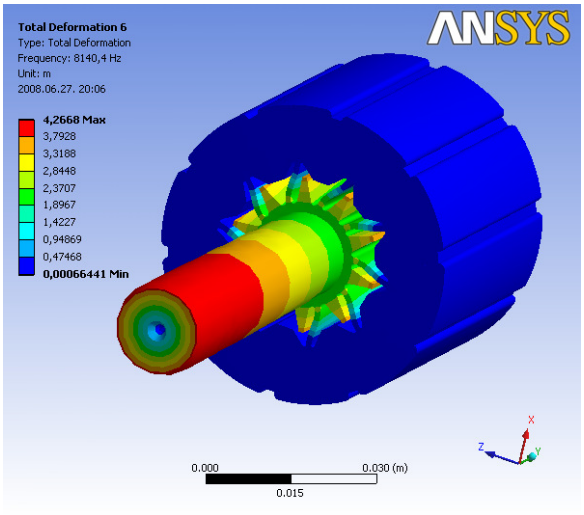

Figure 14: First torsional mode of the rotor. Finite stiffness of bridges, moment of inertia of poles and magnets, and moment of inertia of the shaft produce a resonance at 8140 Hz

In order to complete the motor model presented in Chapter 2, we can build up the rotor by considering two moments of inertia and a torsional spring in between, instead of a single moment of inertia. The conclusion is that if the rotor comes into resonance, the magnitude of the electrical impedance suddenly increases, since at resonance point considerable amount of mechanical energy does oscillate in the system.

Unfortunately, such a high frequency resonance cannot be detected neither in the magnitude, nor in the real part of the impedance due to the inductance considered in the equivalent network.

A possible explanation is that the shaft-end of the motor is fixed for the simulations (see Figure 15). That way the natural frequency of the rotating part will be determined by poles and magnets of much larger moment of inertia (Figure 16).

The conclusions mentioned above are only true if we assume that all cementations of magnets are appropriate, hence the assumption of a bonded, i.e. rigid, contact between poles and magnets is reasonable. In order to simulate potential fabrication problems such as inappropriate bonding of the magnets, the simulations were repeated also with some magnets which were connected to the poles on one side only.

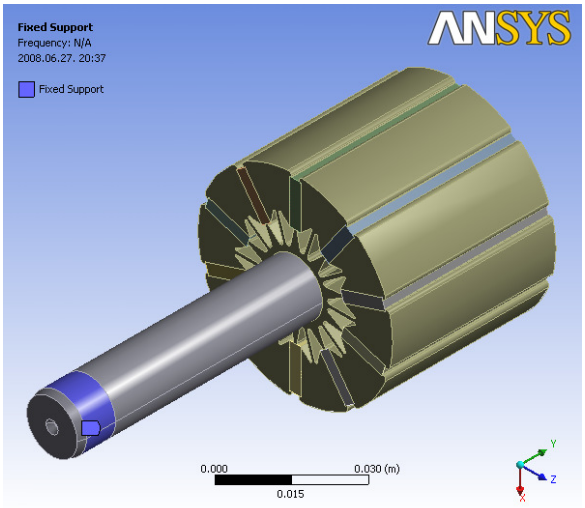

Figure 15: Fixation of the shaft-end in the simulation

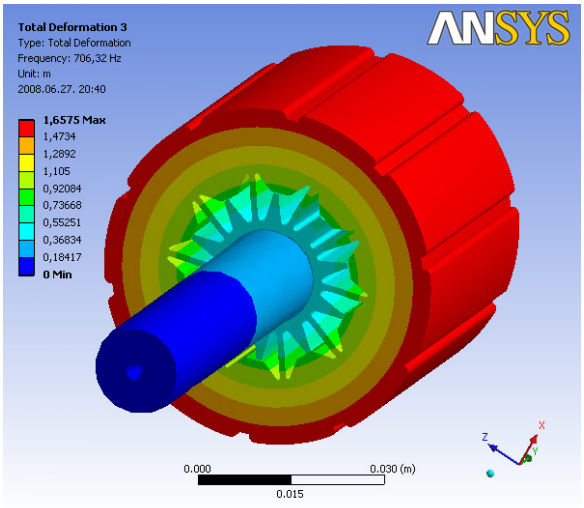

Figure 16: First torsional mode with fixed shaft-end at 706 Hz

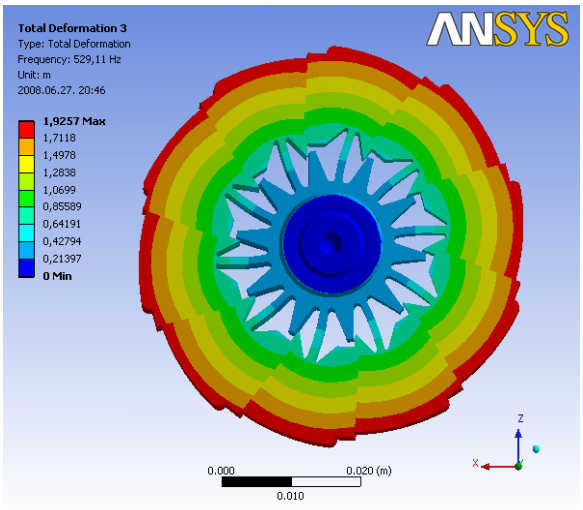

Figure 17: Decreased natural frequency at 529 Hz – cementation is not satisfactory

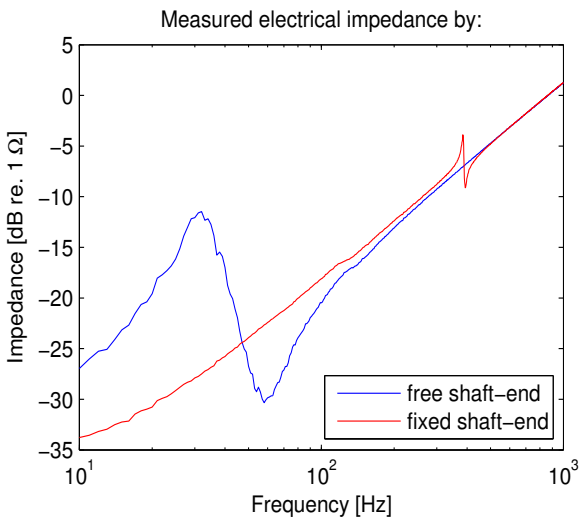

Figure 18: Measured impedance curves by free and fixed shaft-ends

Magnets, in the absence of adhesive on their surface, can move along the poles, hence the natural frequency of the rotor decreases, in this case from the original value of 706 Hz to 529 Hz (Figure 17). If this frequency shift could somehow be detected in the impedance curve, it would be possible to control the quality of the cementation by using a simple impedance measurement.

Figure 18 presents the impedance curve of the earlier introduced ten-pole PMSM in case of free and fixed shaft-end. Due to the fixation the low frequency peak in the impedance curve has disappeared; more precisely, it has shifted to the natural frequency of the rotor. Compared to the calculated 706 Hz natural frequency, the measured 390 Hz is the consequence of finite stiffness of the fixation.

As the motor we have analyzed is in prototype phase (and all of the components are put together uniquely) we have not met a faulty rotor with unsatisfactory cementation, so we have not had the chance to validate the finite element model so far.

5 Summary

The main goal of the works reported herein was to develop a novel vibroacoustic torsional lumped equivalent network of a Permanent Magnet Synchronous Motor (PMSM), which accurately describes the behavior of synchronous machines in the case of pulsating current excitation and small angular displacement of the rotor. First we have introduced an ideal motor model based on physical considerations, than refined it with the vibroacoustic effect of cogging torque. As a result we have gained a model that can be applied in practice reliably.

Furthermore, we presented new measurement techniques for quantifying electrical and mechanical impedances of a PMSM, and have demonstrated for a ten-pole machine that our motor model fitted well to the measured transfer functions, therefore it was possible to estimate the model parameters easily.

Additionally, we revealed a possible practical application of the torsional model for diagnostic purposes. The problem at issue here is quality control of the cementation between the rotor poles and magnets. It was shown by means of numerical simulations, that the natural frequencies of the rotor decrease, when the cementation of the magnets are not satisfactory. We have also shown that as a consequence of the electromagnetic coupling between the electrical and mechanical subsystem of the motor, a shift occurred in the natural frequencies of the torsional system can also be detected in the measured electrical impedance vs frequency functions.

As a summary, we proposed a new method for diagnostic purposes which is based on the idea of exciting torsional systems by using a PMSM as an electro-mechanical transducer. The method opens up new ways to develop fast and reliable testing procedures, which are readily applicable in series production.

Acknowledgements

The results outlined in this paper were achieved with financial, technical, and theoretical support of ThyssenKrupp Presta Hungary Ltd, which is gratefully acknowledged.

References

[1] J. C. Wachel, F. R. Szenasi, *Analysis of torsional vibrations in rotating machinery*, *Proceedings of 22nd Turbomachinery Symposium*, Texas (1993), pp. 127-151.

[2] C. M. Harris, A. G. Piersol, *Shock and Vibration Handbook*, Fifth Edition, McGraw-Hill (2002).

[3] L. Chong-Won, *Vibration Analysis of Rotors*, Kluwer Academic Publishers, Dordrecht / Boston / London (1993).

[4] L. L. Beranek, *Acoustics*, McGraw-Hill Book Company, Inc., New York / Toronto / London (1954).

[5] R H. Small, *Direct-Radiator Loudspeaker System Analysis*, IEEE Transactions on Audio and Electroacoustics, Vol. AU-19, (December 1971), pp. 269-281.

[6] A. N. Thiele, *Loudspeakers in Vented Boxes*, *Proceedings of the IRE Australia*, 22, pp. 487-508 (Augustus 1961); reprinted in Journal of the Audio Eng. Soc., 19, (May 1971), pp. 382-392.

[7] D. Hanselman, *Brushless Permanent Magnet Motor Design*, The Writers' Collective, 2 edition (March 2003).

[8] M. Dai, A. Keyhani, T. Sebastian, *Torque Ripple Analysis of a PM Brushless DC Motor Using Finite Element Method*, IEEE Transactions On Energy Conversion, Vol. 19, No. 1 (March 2004), pp. 40-45.

[9] K. Atallah, J. Wang, D. Howe, *Torque-Ripple Minimization in Modular Permanent-Magnet Brushless Machines*, IEEE Transactions on Industry Applications, Vol. 39, No. 6 (November/December 2003), pp. 1689-1695.

[10] L. Ljung, *System identification: Theory for the User,* Prentice Hall Ptr., Upper Saddle River, NJ, USA (1999).